Scaling phenomena of isobaric yields in projectile fragmentation, spallation, and fission reactions

Chun-Wang Ma (马春旺),* Ling Huang (黄玲), and Yi-Dan Song (宋一丹)
Institute of Particle and Nuclear Physics, Henan Normal University, Xinxiang 453007, China
(Received 10 October 2016; published 21 February 2017)

Background: The isobaric ratio difference scaling phenomenon, which has been found for the fragments produced in projectile fragmentation reactions, is related to the nuclear density change in reaction systems.
Purpose: To verify whether the isobaric ratio difference scaling exists in the fragments produced in the spallation and fission reactions.
Methods: The isobaric ratio difference scaling, denoted by $S_{\Delta \ln R_{21}}$, is in theory deduced within the framework of the canonical ensemble theory at the grand-canonical limitation. The fragments measured in a series of projectile fragmentation, spallation, and fission reactions have been analyzed.
Results: A good $S_{\Delta \ln R_{21}}$ scaling phenomenon is shown for the fragments produced both in the projectile fragmentation reactions and in the spallation reactions, whereas the $S_{\Delta \ln R_{21}}$ scaling phenomenon for the fragments in the fission reaction is less obvious.
Conclusions: The $S_{\Delta \ln R_{21}}$ scaling is used to probe the properties of the equilibrium system at the time of fragment formation. The good scaling of $S_{\Delta \ln R_{21}}$ suggests that the equilibrium state can be achieved in the projectile fragmentation and spallation reactions. Whereas in the fission reaction, the result of $S_{\Delta \ln R_{21}}$ indicates that the equilibrium of the system is hard to achieve.

DOI: 10.1103/PhysRevC.95.024612

I. INTRODUCTION

The isobaric yield ratio of fragments has been used to study the properties of nuclear matter in heavy-ion collisions, which focuses on the nuclear symmetry energy, symmetry energy of a finite nucleus [1–5], temperature of a reaction [6–10], and isospin effects. Based on the isobaric yield ratio, improved methods have been developed to determine the temperature of a system at the chemical freeze-out stage [11,12] and the chemical potential difference of neutrons and protons [13–18]. The isobaric yield ratio difference (IBD) between similar reactions has been found equal to the result of the isoscaling method [13,15]. The IBD method is used to study the change in nuclear density in neutron-rich nuclei [14,16–19]. The scaling phenomenon of information uncertainty for isobars, which have a large difference in neutron excess, has also been found both in the fragments of the measured reactions and the reactions simulated by the asymmetric molecular-dynamics model [20–23]. The isoscaling phenomenon has been found in reactions other than the projectile fragmentation, such as in multifragmentation, evaporation, deeply inelastic reactions [24], spallation [25], and fission [26–28]. Motivated by the isoscaling phenomena in different kinds of reactions, we would like to investigate whether IBD scaling exists in the spallation and fission reactions.

The article is organized as follows. In Sec. II, the IBD scaling is briefly introduced. In Sec. III, with a series of reactions being analyzed, the IBD scaling phenomena for fragments produced in the projectile fragmentation, spallation, and fission reactions are presented and discussed. A brief summary is presented in Sec. IV.

*machunwang@126.com

II. METHOD DESCRIPTION

The canonical ensemble theory is a thermodynamics model. When the system is assumed to be in an equilibrium state, the yields for fragments are decided by the free energy, chemical potential of protons and neutrons, and the temperature of the system. Within the grand canonical limit, the cross section for a fragment is parametrized as [29,30]

$$\sigma(I,A) = CA^{\tau} \exp\{[-F(I,A) + \mu_n N + \mu_p Z]/T\}, \quad (1)$$

where C is a constant, $I \equiv N - Z$ is the neutron excess, T is the temperature, and μ_n (μ_p) is the chemical potential of neutrons (protons), which depends on nuclear density and temperature. $F(I,A)$ is the free energy of a fragment, which also depends on temperature [31,32].

From Eq. (1), the ratio between isobars differing by two units in I can be defined. Taking the logarithm of the ratio, one has

$$\ln R(I+2,I,A) = \ln[\sigma(I+2,A)/\sigma(I,A)]. \quad (2)$$

Inserting Eq. (1) into Eq. (2), one has

$$\ln R(I+2,I,A) = [F(I+2,A) - F(I,A) + \mu_n - \mu_p]/T. \quad (3)$$

For two reactions where the measurement conditions are the same, i.e., the temperatures and the free energies are similar, the IBD between two reactions is defined as [13,15–17]

$$\begin{aligned} &\Delta \ln R_{21}(I+2,I,A) \\ &= \ln[R_2(I+2,I,A)] - \ln[R_1(I+2,I,A)], \\ &= [(\mu_{n2} - \mu_{n1}) - (\mu_{p2} - \mu_{p1})]/T, \end{aligned} \quad (4)$$

in which the free-energy terms cancel out. The indices 2 and 1 denote the neutron-rich system and the more symmetric system, respectively. μ_n (μ_p) is related to the nuclear density

of the system [33], which is used to study the density difference between systems [16,17,21,22]. For simplification, $\Delta\mu_{n21} = \mu_{n2} - \mu_{n1}$ and $\Delta\mu_{p21} = \mu_{p2} - \mu_{p1}$ are defined. Defining the yield ratios between isobars, which have a large differences in (even) I,

$$\Delta \ln R_{21}(I+4,I,A) = 2(\Delta\mu_{n21} - \Delta\mu_{p21})/T, \quad (5)$$

$$\Delta \ln R_{21}(I+6,I,A) = 3(\Delta\mu_{n21} - \Delta\mu_{p21})/T, \quad \cdots = \cdots . \quad (6)$$

Combining Eqs. from (4) to (6), one has

$$S_{\Delta \ln R_{21}} = S_{\Delta \ln R_{21}(I+m,I,A)} = (m/2) \times (\Delta\mu_{n21} - \Delta\mu_{p21})/T, \quad m = 2,4,6,\ldots . \quad (7)$$

$S_{\Delta \ln R_{21}}$ becomes a generalized parameter for fragments with different neutron excesses.

III. RESULTS AND DISCUSSION

A. Projectile fragmentation reactions

The scaling phenomenon of $S_{\Delta \ln R_{21}}$ has been shown for fragments produced in the 140A MeV ^{40,48}Ca (^{58,64}Ni) + ^{9}Be projectile fragmentation reactions [21] in experiments and for the primary fragments and cold fragments in ^{58,64}Ni + ^{9}Be reactions simulated using the antisymmetric molecular-dynamics model plus the sequential decay model GEMINI [21,22]. In this article, the target effect in $S_{\Delta \ln R_{21}}$'s will be studied for the fragments which are produced in ^{40,48}Ca and ^{58,64}Ni + ^{181}Ta /^{9}Be reactions. $S_{\Delta \ln R_{21}}$'s for the symmetric ^{58,64}Ni /^{40}Ca + ^{9}Be, the neutron-rich ^{48}Ca /^{64}Ni + ^{9}Be reactions, and for the ^{58}Ni /^{40}Ca + ^{181}Ta and ^{48}Ca /^{64}Ni + ^{181}Ta reactions will be studied. The cross sections of the fragments are taken from Refs. [34,35]. They have been measured by Mocko *et al.* [35] at the National Superconducting Cyclotron Laboratory, Michigan State University. In addition, the $S_{\Delta \ln R_{21}}$ results for the 1A GeV ^{136}Xe /^{124}Xe + Pb reactions [36], which are larger systems than the Ca and Ni ones, will also be studied.

The results of $S_{\Delta \ln R_{21}}$'s for the fragments in the ^{40}Ca + ^{181}Ta /^{9}Be , ^{48}Ca + ^{181}Ta /^{9}Be , ^{58}Ni + ^{181}Ta /^{9}Be, and ^{64}Ni + ^{181}Ta /^{9}Be reactions have been plotted in Fig. 1. In the ^{40}Ca + ^{181}Ta /^{9}Be reactions, for $m = 2$, I's for the fragments range from -2 to 4; for $m = 4$, I's for the fragments range from -2 to 2; and for $m = 6$, I's for the fragments range from -2 to 0. For most of the fragments, $S_{\Delta \ln R_{21}}$'s are within 0.1 ± 0.3. In the ^{48}Ca + ^{181}Ta /^{9}Be reactions, for $m = 2$, I's for the fragments range from -1 to 11; for $m = 4$, I's for the fragments range from -1 to 9; for $m = 6$, I's for the fragments range from -1 to 7. For most of the fragments, $S_{\Delta \ln R_{21}}$'s are within 0 ± 0.2. In the ^{58}Ni + ^{181}Ta /^{9}Be reactions, for $m = 2$, I's for fragments range from -1 to 7; for $m = 4$, I's for the fragments range from -1 to 5; for $m = 6$, I's for the fragments range from -1 to 3. For most of the fragments, $S_{\Delta \ln R_{21}}$'s are within 0 ± 0.4. In the ^{64}Ni + ^{181}Ta /^{9}Be reactions, for $m = 2$, I's for the fragments range from 0 to 11; for $m = 4$, I's for the fragments range from 0 to 9; for $m = 6$, I's for the fragments range from 0 to 7. For most of the fragments, $S_{\Delta \ln R_{21}}$'s are within the range of 0 ± 0.2. $S_{\Delta \ln R_{21}}$'s for the fragments in the neutron-rich ^{48}Ca and ^{64}Ni reactions show a better scaling phenomenon than that for the symmetric ^{40}Ca and ^{58}Ni reactions. The scaling of $S_{\Delta \ln R_{21}}$ is weakened and disappears when A of the fragments is close to the projectile nucleus.

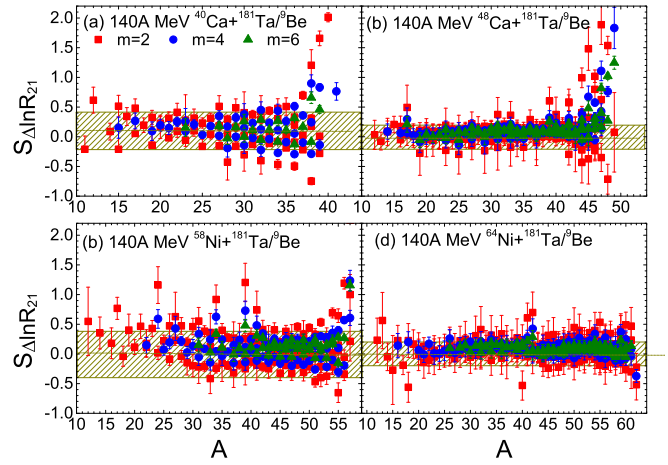

FIG. 1. $S_{\Delta \ln R_{21}}$'s for the fragments produced in the 140A MeV ^{40}Ca + ^{181}Ta /^{9}Be [in (a)], ^{48}Ca + ^{181}Ta /^{9}Be [in (b)], ^{58}Ni + ^{181}Ta /^{9}Be [in (c)], and ^{64}Ni + ^{181}Ta /^{9}Be [in (d)] reactions measured by Mocko *et al.* [34]. m denotes the difference between the I's of the isobars.

$S_{\Delta \ln R_{21}}$'s for fragments produced in the symmetric ^{58}Ni /^{40}Ca + ^{9}Be and the neutron-rich ^{48}Ca /^{64}Ni + ^{9}Be reactions and for the ^{58}Ni /^{40}Ca + ^{181}Ta and ^{48}Ca /^{64}Ni + ^{181}Ta reactions have been plotted in Fig. 2. The $(N/Z)_2/(N/Z)_1$'s for ^{58}Ni /^{40}Ca and ^{48}Ca /^{64}Ni are 1.071 and 1.089, respectively, which are similar. The fragments in the symmetric ^{58}Ni and ^{40}Ca reactions and the neutron-rich ^{40}Ca and

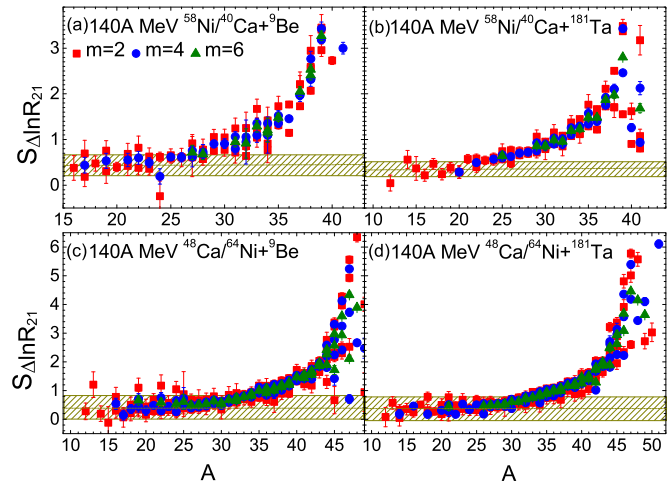

FIG. 2. $S_{\Delta \ln R_{21}}$'s of the fragments produced in the 140A MeV ^{58}Ni /^{40}Ca + ^{9}Be [in (a)], ^{48}Ca /^{64}Ni + ^{9}Be [in (b)], ^{58}Ni /^{40}Ca + ^{181}Ta [in (c)], and ^{48}Ca /^{64}Ni + ^{181}Ta [in (d)] reactions measured by Mocko *et al.* [34]. m denotes the difference between the I's of the isobars.

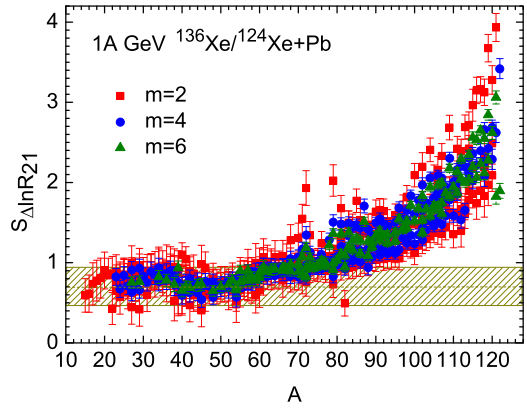

FIG. 3. $S_{\Delta \ln R_{21}}$'s for the fragments produced in the 1A GeV ^{136}Xe /^{124}Xe +Pb reactions measured by Henzlova *et al.* at the FRS-GSI [36]. m denotes the difference between the I's of the isobars.

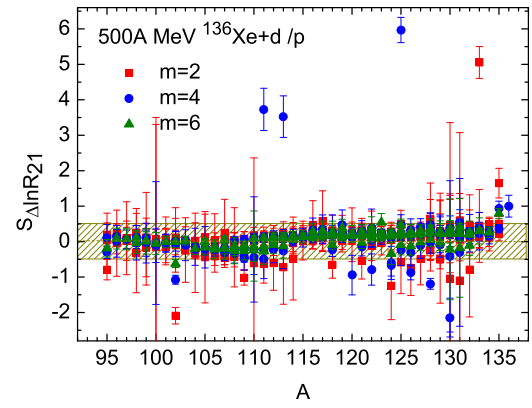

FIG. 4. $S_{\Delta \ln R_{21}}$'s for the fragments produced in the 500A MeV ^{136}Xe +d/p spallation reactions. The cross sections of residue fragments measured in the ^{136}Xe +p and ^{136}Xe +d reactions are taken from Refs. [46,47], respectively. m denotes the difference between the I's of the isobars.

^{64}Ni reactions have been found to be very similar with the same numbers of neutrons or protons abraded from the projectiles, which is interpreted as reflecting the fact that the projectile nuclei have similar neutron or proton density distributions [37]. A good scaling phenomenon of $S_{\Delta \ln R_{21}}$ is found in the symmetric systems ^{58}Ni /^{40}Ca +^{9}Be and can be found in the ^{58}Ni /^{40}Ca +^{181}Ta systems except for the fragments with $A > 37$. Meanwhile, when $A < 43$, a very good scaling of $S_{\Delta \ln R_{21}}$ also is illustrated for the neutron-rich systems ^{48}Ca /^{64}Ni +^{9}Be and ^{48}Ca /^{64}Ni +^{181}Ta. In general, $S_{\Delta \ln R_{21}}$'s for the $m = 2$ fragments have relatively larger fluctuations than those for the $m = 4$ and 6 fragments. In addition, the plateaus of the $S_{\Delta \ln R_{21}}$ distribution cover a narrow mass range with the values of the plateaus being 0.5 ± 0.2, 0.35 ± 0.15, 0.4 ± 0.4, and 0.4 ± 0.4 for the ^{58}Ni /^{40}Ca +^{9}Be , ^{58}Ni /^{40}Ca +^{181}Ta , ^{48}Ca /^{64}Ni +^{9}Be, and ^{48}Ca /^{64}Ni +^{181}Ta systems, respectively.

The yields of fragments with Z ranging from 3 to 56 produced in the 1A GeV ^{136}Xe /^{124}Xe +Pb reactions have been measured by Henzlova *et al.* [36] with a high-resolution magnetic spectrometer, the fragment separator (FRS) of GSI. The IBD results for fragments differing by two units in I have been studied [15]. The values of N/Z for ^{136}Xe /^{124}Xe are 1.519 and 1.296, respectively, with $(N/Z)_2/(N/Z)_1$ being 1.171. $S_{\Delta \ln R_{21}}$'s for the measured fragments in the ^{136}Xe /^{124}Xe +Pb reactions are plotted in Fig. 3. For $m = 2$, I's for the fragments range from -1 to 17; for $m = 4$, I's for the fragments range from -1 to 15; and for $m = 6$, I's for fragments range from -1 to 13. For fragments of $A < 60$, $S_{\Delta \ln R_{21}}$ is within 0.8 ± 0.3. When $A > 60$, $S_{\Delta \ln R_{21}}$ increases slowly. Meanwhile, $S_{\Delta \ln R_{21}}$'s show better scaling phenomena for fragments of $A < 60$ than those for $A > 60$. $S_{\Delta \ln R_{21}}$'s for $m = 2$ have a relatively wider range than those for $m = 4$ and 6, indicating that the fragments are better scaled when m is large. From the $S_{\Delta \ln R_{21}}$ distributions shown in Figs. 1–3, we conclude that the plateau of $S_{\Delta \ln R_{21}}$ is determined mainly by the difference between the isospins of the projectile nuclei.

In the projectile fragmentation reactions, the $S_{\Delta \ln R_{21}}$ scaling phenomenon has been found, especially for the system of similar isospin. For isobars produced in the relatively large reaction systems, some peaks can be found in the $S_{\Delta \ln R_{21}}$ distributions for the isobars differing by $m = 2$ or 4. This is due to the shell evolution as that in the IBD results for the $m = 2$ isobars [15].

B. Spallation reactions

Spallation reactions are induced by nucleons or light projectiles from a few hundred MeV/u to the relativistic domain. At incident energies of a few hundred MeV/u, the system can be described as a fast excitation followed by a slower decay process [38,39] of evaporation and fission, depending on the phase space of the system [40,41]. In the spallation reaction at relativistic energies, the studies using the thermodynamic observable found that the liquid-gas phase transition and multifragmentation process can be connected to each other [42–45].

The residual fragments in the 500A MeV ^{136}Xe +p and 500A MeV ^{136}Xe +d spallation reactions have been measured by Giot *et al.* [46] and Alcántara-Núñez *et al.* [47], respectively, at the FRS-GSI (Darmstadt). For convenience, the spallation nucleus ^{136}Xe is called the parent nucleus of the system. The results of $S_{\Delta \ln R_{21}}$'s for the fragments have been plotted in Fig. 4. For $m = 2$, I's of the fragments range from 7 to 29; for $m = 4$, I's of the fragments range from 7 to 27; for $m = 6$, I's of the fragments range from 7 to 25. For most of the fragments, $S_{\Delta \ln R_{21}}$'s are within 0 ± 0.5. A large staggering is found in $S_{\Delta \ln R_{21}}$'s for the $m = 2$ and 4 distributions. From $m = 2$ to 6, the range of $S_{\Delta \ln R_{21}}$'s becomes narrower and shows a better scaling.

The fragments produced in the 1A GeV ^{238}U +p and ^{136}Xe +p spallation reactions have been measured by Taïeb *et al.* [48] and Napolitani *et al.* [49], respectively, at the FRS-GSI (Darmstadt). The values of N/Z for ^{238}U and ^{136}Xe are 1.587 and 1.519, respectively, with $(N/Z)_2/(N/Z)_1$ being 1.045. The $S_{\Delta \ln R_{21}}$'s for the residues of the 1A GeV ^{136}Xe /^{238}U +p spallation reactions are plotted in Fig. 5. For $m = 2$, I's of the fragments range from 4 to 28; for $m = 4$, I's of the fragments range from 4 to 26; and for

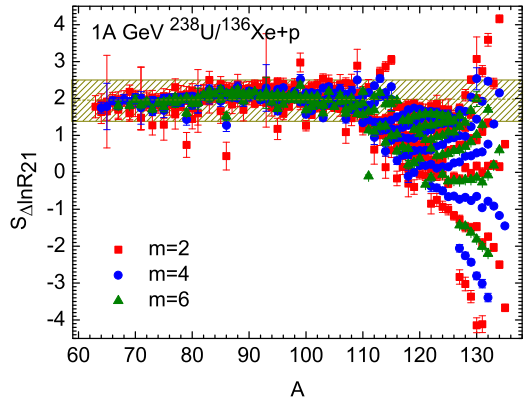

FIG. 5. $S_{\Delta \ln R_{21}}$'s for the fragments produced in the 1A GeV ^{238}U$/^{136}$Xe$+p$ spallation reactions. The cross sections of the fragments measured in the ^{238}U$+p$ and ^{136}Xe$+p$ reactions are taken from Refs. [48,49], respectively. m denotes the difference between I's of the isobars.

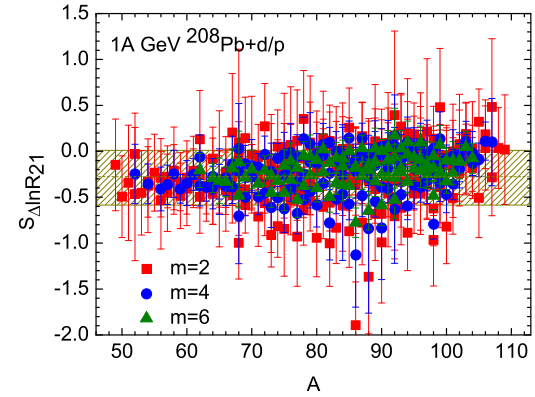

FIG. 7. $S_{\Delta \ln R_{21}}$'s for the fragments produced in the 1A GeV ^{208}Pb$+d/p$ fission reactions. The cross section of fragments measured in the 1A GeV ^{208}Pb$+d$ and ^{208}Pb$+p$ reactions are taken from Refs. [52,53], respectively. m denotes the difference between the I's of the isobars.

$m = 6$, I's of the fragments range from 5 to 24. The $S_{\Delta \ln R_{21}}$'s for the $m = 2$ fragments have a wider range than those for the $m = 4$ and 6 fragments. The $S_{\Delta \ln R_{21}}$'s for the fragments are within 2.0 ± 0.5 in the range of $A < 115$, which shows a good scaling phenomenon. But the $S_{\Delta \ln R_{21}}$ has a much wider range for the fragment of $A > 115$, indicating that the scaling phenomenon is weakened and disappears.

The fragments produced in the 1A GeV ^{136}Xe$+p$ and ^{56}Fe$+p$ spallation reactions have been measured by Napolitani *et al.* [49] and Villagrasa-Canton *et al.* [50], respectively, at the FRS-GSI (Darmstadt). The values of N/Z for ^{136}Xe and ^{56}Fe are 1.519 and 1.154, respectively, with $(N/Z)_2/(N/Z)_1$ being 1.316. $S_{\Delta \ln R_{21}}$'s for the fragments in the 1A GeV ^{136}Xe$/^{56}$Fe$+p$ spallation reactions are plotted in Fig. 6. For $m = 2$, I's of the fragments range from -1 to 6; for $m = 4$, I's of the fragments range from -1 to 4; and for $m = 6$, I's of the fragments range from 0 to 2. In a wide range of A ($A < 45$), $S_{\Delta \ln R_{21}}$'s for $m = 2$, 4, and 6 are within 1.8 ± 0.4. A relatively large range of $S_{\Delta \ln R_{21}}$ is shown for the $A > 45$ fragments. From $m = 2$ to 6, the staggering in $S_{\Delta \ln R_{21}}$'s is weakened, showing a better scaling phenomenon.

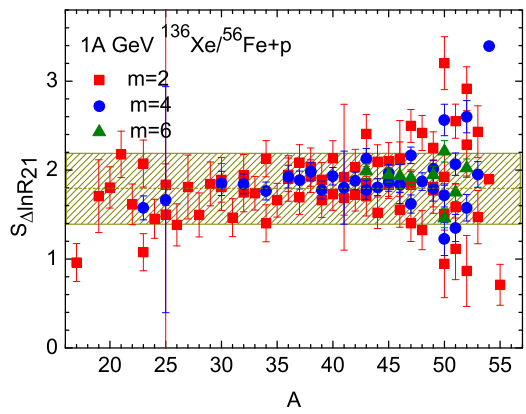

FIG. 6. $S_{\Delta \ln R_{21}}$'s for the fragments produced in the 1A GeV ^{136}Xe$/^{56}$Fe$+p$ spallation reactions. The cross sections of the fragments in the 1A GeV ^{136}Xe$+p$ and ^{56}Fe$+p$ reactions are taken from Refs. [49,50], respectively. m denotes the difference between the I's of the isobars.

In the spallation reactions, except those comparable to that of the parent nucleus, the $S_{\Delta \ln R_{21}}$'s also show good scaling. Meanwhile, some maximum and minimum peaks have been found in the $S_{\Delta \ln R_{21}}$ distribution for the $m = 2$ and 4 fragments. This can be explained by the shell evolution in the neutron-rich fragments [15].

C. Fission reactions

Fission is one of the methods employed to produce new isotopes. The fissile fragments from a heavy nucleus source with an excitation energy close to the fission barrier decays at reactions of high collision energy. The increase in excitation energy forces light particle emission, which reduces the probability of fission. The competition between the decay channels provides keys for understanding the properties of hot nuclei, such as the structure, the level density, and the shell evolution with excitation energy [51].

The fissile fragments of 1A GeV ^{208}Pb$+d$ [52] and ^{208}Pb$+p$ [53] reactions have been measured by Enqvist *et al.* [52] at the FRS-GSI (Darmstadt). $S_{\Delta \ln R_{21}}$'s for the fragments of the 1A GeV ^{208}Pb$+d/p$ fission reactions have been studied and plotted in Fig. 7. For $m = 2$, I's of the fragments range from 3 to 19; for $m = 4$, I's of the fragments range from 4 to 17; for $m = 6$, I's of the fragments range from 4 to 14. For the fragments of $A < 65$, the $S_{\Delta \ln R_{21}}$ distributions for $m = 2$, 4, and 6 are within 0.3 ± 0.3, showing a good scaling phenomenon, but for fragments of $A > 65$, $S_{\Delta \ln R_{21}}$'s for the $m = 2$ and 4 spreads to a much wider range.

The fragments produced in the 1A GeV ^{238}U$+d$ and ^{238}U$+p$ fission reactions have been measured by Pereira *et al.* [54] and Bernas *et al.* [51], respectively, at the FRS-GSI (Darmstadt). $S_{\Delta \ln R_{21}}$'s for the fragments in the 1A GeV ^{238}U$+d/p$ fission reactions are plotted in Fig. 8. For $m = 2$, I's of the fragments range from 4 to 34; for $m = 4$, I's of the fragments range from 4 to 32; and for $m = 6$, I's of the fragments range from 5 to 30. From $m = 2$ to 6, the

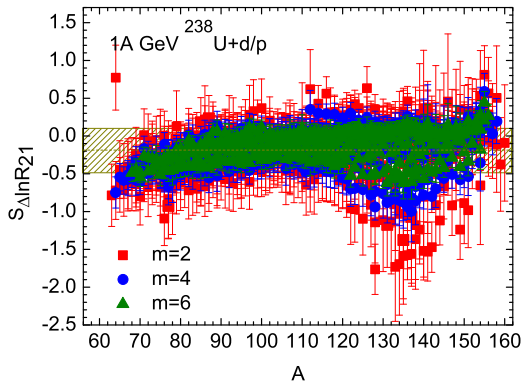

FIG. 8. $S_{\Delta \ln R_{21}}$'s for the fragments produced in the 1A GeV ^{238}U$+d/p$ fission reactions. The cross sections of the fragments measured in the 1A GeV ^{238}U$+d$ and ^{238}U$+p$ reactions are taken from Refs. [51,54], respectively. m denotes the difference between the I's of the isobars.

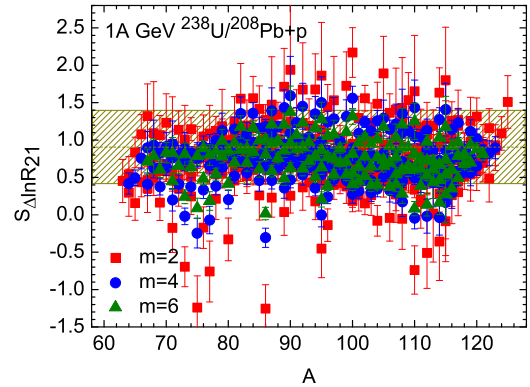

FIG. 9. $S_{\Delta \ln R_{21}}$'s for the fragments produced in the 1A GeV ^{238}U$/^{208}$Pb$+p$ fission reactions. The cross sections of the fragments measured in the 1A GeV ^{238}U$+p$ and ^{208}Pb$+p$ reactions are taken from Refs. [51,53], respectively. m denotes the difference between the I's of the isobars.

range of $S_{\Delta \ln R_{21}}$'s becomes narrower. For fragments of $A < 120$, $S_{\Delta \ln R_{21}}$'s show good scaling phenomena for $m = 2$, 4, and 6, most of which are within the range of -0.2 ± 0.3. A relatively large range of $S_{\Delta \ln R_{21}}$ is shown for the $A > 120$ fragments.

$S_{\Delta \ln R_{21}}$'s for the fissile fragments in the 1A GeV ^{238}U$/^{208}$Pb$+p$ reactions are plotted in Fig. 9. For $m = 2$, I's of the fragments range from 4 to 21; for $m = 4$, I's of the fragments range from 4 to 19; for $m = 6$, I's of the fragments range from 5 to 17. For most of the fragments, although $S_{\Delta \ln R_{21}}$'s are within 0.9 ± 0.5, large fluctuations have been observed in the results, indicating that $S_{\Delta \ln R_{21}}$'s for the fragments are not well scaled.

The $S_{\Delta \ln R_{21}}$ scaling for the fissile fragments has been studied by analyzing the measured data. The $S_{\Delta \ln R_{21}}$ scaling for the fissile fragments is not as good as those for the fragments produced in the projectile fragmentation and spallation reactions.

IV. SUMMARY

The $S_{\Delta \ln R_{21}}$ scaling phenomenon, denoted by the similar distributions for isobars differing by units of neutron excess, has been studied by investigating the residue fragments in a series of reactions including projectile fragmentation, spallation, and fission reactions. The typical scaling of $S_{\Delta \ln R_{21}}$ shows the consistent distributions for isobars which have different neutron excesses. The height for the plateau of $S_{\Delta \ln R_{21}}$ is found to depend on the isospin of the projectile nucleus. A good $S_{\Delta \ln R_{21}}$ scaling has been found for the measured fragments, both in the projectile fragmentation reactions and in the spallation reactions, whereas the scaling of $S_{\Delta \ln R_{21}}$ for the fissile fragment is not well illustrated.

The scaling of $S_{\Delta \ln R_{21}}$ is deduced from the canonical ensemble theory, which assumes the system is in an equilibrium state. The scaling of $S_{\Delta \ln R_{21}}$ is observed for the fragments with mass numbers much smaller than the projectile nucleus or the parent nucleus of the spallation reaction. It can be concluded that, except for the fragments which have the relatively large mass numbers, the equilibrium state can be assumed in the projectile fragmentation and spallation reactions. For fragments produced in the systems with similar isospins, a quite good scaling of $S_{\Delta \ln R_{21}}$ can be found for almost all of the fragments, indicating that they have similar nuclear (neutron or proton) density distributions.

ACKNOWLEDGMENTS

This work was supported by the Program for Science and Technology Innovation Talents at the Universities of Henan Province (Grant No. 13HASTIT046), the Natural and Science Foundation in Henan Province (Grant No. 162300410179), and the Program for the Excellent Youth (Grant No. 154100510007) at Henan Normal University.

[1] C.-W. Ma, F. Wang, Y.-G. Ma, and C. Jin, Phys. Rev. C **83**, 064620 (2011).
[2] C. W. Ma, J. B. Yang, M. Yu *et al.*, Chin. Phys. Lett. **29**, 092101 (2012).
[3] C.-W. Ma *et al.*, Eur. Phys. J. A **48**, 78 (2012).
[4] C.-W. Ma, J. Pu, S.-S. Wang, and H.-L. Wei, Chin. Phys. Lett. **29**, 062101 (2012).
[5] C.-W. Ma *et al.*, Chin. Phys. C **37**, 024101 (2013).
[6] C.-W. Ma, C.-Y. Qiao, T.-T. Ding, and Y.-D. Song, Nucl. Sci. Tech. **27**, 111 (2016).
[7] C.-W. Ma, J. Pu, Y. G. Ma, R. Wada, and S. S. Wang, Phys. Rev. C **86**, 054611 (2012).
[8] C.-W. Ma, X.-L. Zhao, J. Pu, S.-S. Wang, C.-Y. Qiao, X. Feng, R. Wada, and Y.-G. Ma, Phys. Rev. C **88**, 014609 (2013).
[9] C. Ma, C. Qiao, S. Wang, F. Lu, L. Chen, and M. Guo, Nucl. Sci. Tech. **24**, 050510 (2013).
[10] X.-Q. Liu, M.-R. Huang, R. Wada *et al.*, Nucl. Sci. Tech. **25**, S20508 (2015).
[11] C.-W. Ma, T.-T. Ding, C.-Y. Qiao, and X.-G. Cao, Phys. Rev. C **92**, 064601 (2015).

[12] T.-T. Ding and C.-W. Ma, Nucl. Sci. Tech. **27**, 142 (2016).
[13] C. W. Ma, S. S. Wang, Y. L. Zhang, and H. L. Wei, Phys. Rev. C **87**, 034618 (2013).
[14] C.-W. Ma, Y.-L. Zhang, C.-Y. Qiao, and S.-S. Wang, Phys. Rev. C **91**, 014615 (2015).
[15] C. W. Ma, S. S. Wang, Y. L. Zhang, and H. L. Wei, J. Phys. G: Nucl. Part. Phys. **40**, 125106 (2013).
[16] C. W. Ma, J. Yu, X. M. Bai, Y. L. Zhang, H. L. Wei, and S. S. Wang, Phys. Rev. C **89**, 057602 (2014).
[17] C. W. Ma, X. M. Bai, J. Yu, and H. L. Wei, Eur. Phys. J. A **50**, 139 (2014).
[18] M. Yu, K.-J. Duan, S.-S. Wang, Y.-L. Zhang, and C.-W. Ma, Nucl. Sci. Tech. **26**, S20503 (2015).
[19] C. Y. Qiao, H. L. Wei, C. W. Ma, Y. L. Zhang, and S. S. Wang, Phys. Rev. C **92**, 014612 (2015).
[20] C. W. Ma and H. L. Wei, Commun. Theor. Phys. **62**, 717 (2014).
[21] C. W. Ma *et al.*, Phys. Lett. B **742**, 19 (2015).
[22] C.-W. Ma *et al.*, J. Phys. G: Nucl. Part. Phys. **43**, 045102 (2016).
[23] M. Huang *et al.*, Nucl. Phys. **A847**, 233 (2011).
[24] M. B. Tsang, W. A. Friedman, C. K. Gelbke, W. G. Lynch, G. Verde, and H. S. Xu, Phys. Rev. Lett. **86**, 5023 (2001).
[25] M. N. Andronenko, L. N. Andronenko, and W. Neubert, Eur. Phys. J. A **31**, 125 (2007).
[26] M. Veselsky, G. A. Souliotis, and M. Jandel, Phys. Rev. C **69**, 044607 (2004).
[27] W. A. Friedman, Phys. Rev. C **69**, 031601(R) (2004).
[28] Y. G. Ma *et al.*, Phys. Rev. C **72**, 064603 (2005).
[29] C. B. Das, S. Das Gupta, X. D. Liu, and M. B. Tsang, Phys. Rev. C **64**, 044608 (2001).
[30] M. B. Tsang *et al.*, Phys. Rev. C **76**, 041302(R) (2007).
[31] S. J. Lee and A. Z. Mekjian, Phys. Rev. C **82**, 064319 (2010).
[32] C.-W. Ma, F. Niu, C.-Y. Qiao, Y.-F. Niu, and T.-Z. Yan, Phys. Rev. C **94**, 024615 (2016).
[33] E. Geraci, M. Bruno, and M. D'Agostino, Nucl. Phys. **A732**, 173 (2004).
[34] M. Mocko *et al.*, Phys. Rev. C **74**, 054612 (2006).
[35] M. Mocko, Doctorial thesis, Michigan State University, 2006.
[36] D. Henzlova *et al.*, Phys. Rev. C **78**, 044616 (2008).
[37] C.-W. Ma *et al.*, Phys. Rev. C **79**, 034606 (2009).
[38] T. D. Thomas, Annu. Rev. Nucl. Part. Sci. **18**, 343 (1968).
[39] S. J. Sanders, A. S. de Toledo, and C. Beck, Phys. Rep. **311**, 487 (1999).
[40] U. L. Businaro and S. Gallone, Nuovo Cimento **1**, 629 (1955).
[41] U. L. Businaro and S. Gallone, Nuovo Cimento **1**, 1277 (1955).
[42] V. E. Viola *et al.*, Phys. Rep. **434**, 1 (2006).
[43] A. S. Botvina, A. S. Iljinov, and I. N. Mishustin, Nucl. Phys. **A507**, 649 (1990).
[44] V. A. Karnaukhov, Phys. At. Nucl. **66**, 1242 (2003).
[45] P. Napolitani and M. Colonna, Phys. Rev. C **92**, 034607 (2015).
[46] L. Giot, J. A. Alcántara-Núñez, J. Benlliure *et al.*, Nucl. Phys. **A899**, 116 (2013).
[47] J. A. Alcántara-Núñez, J. Benlliure, C. Paradela *et al.*, Phys. Rev. C **92**, 024607 (2015).
[48] J. Taïeb, K.-H. Schmidt, L. Tassan-Got *et al.*, Nucl. Phys. **A724**, 413 (2003).
[49] P. Napolitani, K.-H. Schmidt, L. Tassan-Got *et al.*, Phys. Rev. C **76**, 064609 (2007).
[50] C. Villagrasa-Canton, A. Boudard, J.-E. Ducret *et al.*, Phys. Rev. C **75**, 044603 (2007).
[51] M. Bernas, P. Armbruster, J. Benlliure *et al.*, Nucl. Phys. **A725**, 213 (2003).
[52] T. Enqvist, W. Wlazłob, P. Armbruster *et al.*, Nucl. Phys. **A686**, 481 (2001).
[53] T. Enqvist, P. Armbruster, J. Benlliure *et al.*, Nucl. Phys. **A703**, 435 (2002).
[54] J. Pereira, J. Benlliure, E. Casarejos *et al.*, Phys. Rev. C **75**, 014602 (2007).